*Inorg. Chem.* **2006**, *45*, 8500–8508


# Metal-Binding Thermodynamics of the Histidine-Rich Sequence from the Metal-Transport Protein IRT1 of *Arabidopsis thaliana*

**Nicholas E. Grossoehme,[†] Shreeram Akilesh,[†,‡] Mary Lou Guerinot,[‡] and Dean E. Wilcox*[,†]**

*Departments of Chemistry and Biological Sciences, Dartmouth College, Hanover, New Hampshire 03755*

Received April 14, 2006

The widespread ZIP family of transmembrane metal-transporting proteins is characterized by a large intracellular loop that contains a histidine-rich sequence whose biological role is unknown. To provide a chemical basis for this role, we prepared and studied a peptide corresponding to this sequence from the first iron-regulated transporter (IRT1) of *Arabidopsis thaliana*, which transports $Fe^{2+}$ as well as $Mn^{2+}$, $Co^{2+}$, $Zn^{2+}$, and $Cd^{2+}$. Isothermal titration calorimetry (ITC) measurements, which required novel experiments and data analysis, and supporting spectroscopic methods were used to quantify IRT1's metal-binding affinity and associated thermodynamics. The peptide, PHGHGHGHGP, binds metal ions with 1:1 stoichiometry and stabilities that are consistent with the Irving–Williams series. Comparison of the metal-binding thermodynamics of the peptide with those of trien provides new insight about enthalpic and entropic contributions to the stability of the metal–peptide complex. Although $Fe^{2+}$ and other IRT1-transported metal ions do not bind very tightly, this His-rich sequence has a very high entropy-driven affinity for $Fe^{3+}$, which may have biological significance.

## Introduction

Trace elements are often limiting nutrients for the growth of plants, which make a substantial genetic and biochemical investment to obtain iron and other essential metals from soil. Two general mechanisms are known for iron uptake into root cells by plants.[1−3] Grasses employ a Strategy II mechanism, in which siderophores are excreted into the soil, where they form very stable complexes with $Fe^{3+}$ that are recognized by cell surface receptors and transported into the cell. Most plants, however, use a Strategy I mechanism, in which three membrane proteins are required to import iron.[4] An ATPase pumps protons into the soil to lower the pH and solubilize ferric ions that are reduced by an NADH-dependent reductase and the resulting ferrous ions are then transported into the cell. Recent evidence, though, suggests that the Strategy II plant rice possesses an $Fe^{2+}$ uptake mechanism as well.[5]

A significant advance in understanding the Strategy I mechanism was the discovery of the first iron-regulated transporter (IRT1) of *Arabidopsis thaliana*.[6] This high-affinity iron-transport protein found in the outer membrane of root cells[7] was the founding member of the widespread ZIP (ZRT- and IRT-like proteins) family of metal transporters. Proteins in this family import a number of essential metals and are characterized by their localization to various cellular membranes, eight putative membrane-spanning helices, and a long intracellular loop between helices 3 and 4 that contains a histidine-rich sequence.[8]

Uptake studies of IRT1, either in *A. thaliana*[7] or expressed in yeast,[6,9] have shown that $Mn^{2+}$, $Zn^{2+}$, $Cd^{2+}$, and $Co^{2+}$, in addition to $Fe^{2+}$, are transported and that $Fe^{2+}$ transport is competitively inhibited by $Cd^{2+}$,[6] whereas $Mn^{2+}$ uptake is inhibited by $Fe^{2+}$, $Cu^{2+}$, $Zn^{2+}$, and $Cd^{2+}$ and $Zn^{2+}$ uptake is

* To whom correspondence should be addressed. E-mail: dean.wilcox@dartmouth.edu. Phone: 603-646-2874.
† Department of Chemistry, Dartmouth College.
‡ Department of Biological Sciences, Dartmouth College.

(1) Staiger, D. *Angew. Chem., Int. Ed.* **2002**, *41*, 2259−2264.
(2) Schmidt, W. *J. Plant Nutr.* **2003**, *26*, 2211−2230.
(3) Curie, C.; Briat, J. F. *Annu. Rev. Plant Biol.* **2003**, *54*, 183−206.
(4) Grotz, N.; Guerinot, M. L. *Curr. Opin. Plant Biol.* **2002**, *5*, 158−163.
(5) Ishimaru, Y.; Suzuki, M.; Tsukamoto, T.; Suzuki, K.; Nakazono, M.; Kobayashi, T.; Wada, Y.; Watanabe, S.; Matsuhashi, S.; Takahashi, M.; Nakanishi, H.; Mori, S.; Nishizawa Naoko, K. *Plant J.* **2006**, *45*, 335−346.
(6) Eide, D.; Broderius, M.; Fett, J.; Guerinot, M. L. *Proc. Natl. Acad. Sci. U.S.A.* **1996**, *93*, 5624−5628.
(7) Vert, G.; Grotz, N.; Dedaldechamp, F.; Gaymard, F.; Guerinot, M. L.; Briata, J. F.; Curie, C. *Plant Cell* **2002**, *14*, 1223−1233.
(8) Guerinot, M. L. *Biochim. Biophys. Acta* **2000**, *1465*, 190−198.
(9) Korshunova, Y. O.; Eide, D.; Clark, W. G.; Guerinot, M. L.; Pakrasi, H. B. *Plant Mol. Biol.* **1999**, *40*, 37−44.



10.1021/ic0606431 CCC: $33.50 
Published on Web 08/03/2006

inhibited by $Cd^{2+}$, $Co^{2+}$, and $Fe^{3+}$.[9] Mutagenesis studies have identified several residues on the extracellular side of the protein and in the transmembrane helices that are crucial for iron uptake and/or modulating the metal-transport specificity.[10]

Histidine-rich sequences are not limited to metal transporters in the ZIP family, as they are also present in the cation diffusion facilitator (CDF) family[11] and ABC metal transporters.[12,13] However, the role of these characteristic sequences, which for IRT1 is PHGHGHGHGP, is still unknown. In the case of ZRT1 (zinc-regulated transporter), the high-affinity zinc transporter in yeast, the mutation of each histidine in its sequence (HDHTHDE) to glutamine did not significantly effect $K_m$ for $Zn^{2+}$ uptake but dramatically reduced $V_{max}$; this may, however, have resulted from reduced protein localization to the plasma membrane.[14] Similar metal-uptake studies of an IRT1 mutant with its four histidines replaced by glutamines have demonstrated that the His residues are not necessary for $Fe^{2+}$ or $Zn^{2+}$ uptake.[15]

To provide a chemical basis for the role of the omnipresent His-rich sequences in the ZIP family, we have used isothermal titration calorimetry (ITC) to quantify the metal-binding affinity and associated thermodynamics of a peptide corresponding to the IRT1 sequence. This required novel calorimetric experiments and data analysis and supporting spectroscopic measurements. We find that metal ions generally bind with 1:1 stoichiometry and that the first-row transition-metal ions from $Mn^{2+}$ to $Zn^{2+}$ bind with relative stabilities consistent with the Irving−Williams series. Although higher metal affinity does not correlate with ions that are transported, these results quantify the interaction of these intracellular His-rich sequences with metal ions, particularly those imported by IRT1 and other members of the ZIP family. Further, these results provide useful insight about the metal binding properties of other His-rich protein sequences associated with metallobiochemistry[16] and diseases such as malaria.[17,18]

## Experimental Section

The N-acetylated and C-amidated IRT1 peptide (IRT1pep), PHGHGHGHGP, was obtained from BioSynthesis and further purified to >97% by reverse-phase HPLC on a VYDAC C18 column with a 0−70% acetonitrile (Fisher, HPLC grade) gradient containing 0.1% TFA (Acros). All reagents were the highest purity available (≥99%) and used as received. All metal ions were obtained as chloride or sulfate salts from either Fisher or Sigma. *N*-(2-hydroxyethyl)piperazine-N′-(2-ethanesulfonic acid) (HEPES), piperazine-*N*,*N*′-bis(2-ethanesulfonic acid) (PIPES), 2-amino-2-(hyroxymethyl)-1,3-propanediol (Tris), and ethylenediaminetetraacetic acid (EDTA) were obtained from Sigma, whereas 3-(*N*-morpholino)propanesulfonic acid (MOPS), *N*-(2-acetamido)-2-aminoethanesulfonic acid (ACES), triethylenetetramine (trien), and sodium dithionite were obtained from Fisher.

Isothermal titration calorimetry (ITC) experiments were carried out at 25.0 (±0.2) °C on either a MicroCal MCS or VP microcalorimeter, as described previously.[19] No systematic differences between results from the two calorimeters were observed. Anaerobic measurements were conducted under a $N_2$ or Ar atmosphere in custom-built Plexiglass gloveboxes that enclosed the calorimeters. IRT1pep samples were prepared in 25 mM ACES, HEPES, MOPS, or PIPES buffer at pH 7.25 or 100 mM Tris buffer at pH 8.22, with the ionic strength adjusted to 100 mM with NaCl. $Fe^{2+}$ and $Mn^{2+}$ solutions were prepared under anaerobic conditions and thoroughly deoxygenated before experiments were carried out. For experiments involving $Fe^{2+}$, 50 $\mu$M sodium dithionite ($Na_2S_2O_4$) was added to both the peptide and the $Fe^{2+}$ solutions to eliminate oxidation by any trace $O_2$. Low stability of the $Fe^{2+}$−peptide complex necessitated the need for four successive syringe volumes to titrate the IRTpep solutions. The raw data sets were concatenated to account for dilution and provide a complete reaction profile. Stock metal solutions were standardized by ITC with a metal−EDTA titration. The concentration of stock peptide solutions was initially determined gravimetrically, using 1596 g/mol as the molar mass of the peptide and five TFA anions, followed by an ITC titration with a standardized $Zn^{2+}$ solution.

A minimum of two, and typically three, titrations were carried out for each metal, and the reported experimental values are the average of individual best-fit values, determined with either the one-site or sequential binding model in the Origin software package, version 7.0. ITC results are presented by showing baseline-adjusted experimental titration data (heat flow versus time) on the top and peak-integrated background-subtracted concentration-normalized molar heat flow per aliquot versus the titrant-to-sample molar ratio on the bottom. The change in free energy for the overall equilibrium of each ITC titration, $\Delta G_{overall}$, was determined from the equilibrium constant obtained from the best fit of the experimental data, $K_{ITC}$

$$\Delta G_{overall} = \Delta G_{ITC} = -RT \ln K_{ITC} \quad (1)$$

as will be discussed in more detail elsewhere.[20]

Electron paramagnetic resonance (EPR) measurements were carried out on a Brüker EMX-300 spectrometer. Samples were prepared and incubated for 1 h at room temperature before immersion into liquid nitrogen. $Mn^{2+}$ samples were prepared under an inert atmosphere. EPR spectra were collected at 77 K using a 100 kHz modulation frequency, a modulation amplitude of 1.0 G for $Mn^{2+}$ and 10.0 G for $Cu^{2+}$, and a 10 ms time constant. Data were manipulated and analyzed with the WINEPR software provided by Brüker.

An AccuMet pH meter was used to monitor pH titrations, which were carried out with 1.0 $\mu$L injections of 0.100 M NaOH into 1.0 mL of 1.25 $\mu$M IRT1pep. Data were fit using the Origin nonlinear curve-fitting feature according to the algorithm

(10) Rogers, E. E.; Eide, D. J.; Guerinot, M. L. *Proc. Natl. Acad. Sci. U.S.A.* **2000**, *97*, 12356−12360.
(11) Hall, J. L.; Williams, L. E. *J. Exp. Bot.* **2003**, *54*, 2601−2613.
(12) Williams, L. E.; Pittman, J. K.; Hall, J. L. *Biochim. Biophys. Acta* **2000**, *1465*, 104−126.
(13) Li, L.; Kaplan, J. *J. Biol. Chem.* **1997**, *272*, 28485−28493.
(14) Gitan, R. S.; Shababi, M.; Kramer, M.; Eide, D. J. *J. Biol. Chem.* **2003**, *278*, 39558−39564.
(15) Connolly, E. L. 2006, personal communication.
(16) Colpas, G. J.; Brayman, T. G.; Ming, L. J.; Hausinger, R. P. *Biochemisty* **1999**, *38*, 4078−4088.
(17) Pandey, A. V.; Bisht, H.; Babbarwal, V. K.; Srivastava, J.; Pandey, K. C.; Chauhan, V. S. *Biochem. J.* **2001**, *355*, 333−338.
(18) Kilejian, A. *Science* **1978**, *201*, 922−924.
(19) Zhang, Y.; Akilesh, S.; Wilcox, D. E. *Inorg. Chem.* **2000**, *39*, 3057−3064.
(20) Spuches, A. M.; Grossoehme, N. E.; Elgren, T. E.; Wilcox, D. E. In preparation.

$$V_B = \frac{V_L\left\{C'_L\left(\frac{6}{1+K_{HTFA}[H^+]} - \frac{\alpha}{Q}\right) + K_w[H^+]^{-1} - [H^+]\right\}}{C_B - K_w[H^+]^{-1} + [H^+]} \quad (2)$$

$$\alpha = 5\beta_{5,HL}[H]^5 + 4\beta_{4,HL}[H]^4 + 3\beta_{3,HL}[H]^3 + 2\beta_{2,HL}[H]^2 + K_{1,HL}[H]$$

$$Q = 1 + \beta_{5,HL}[H]^5 + \beta_{4,HL}[H]^4 + \beta_{3,HL}[H]^3 + \beta_{2,HL}[H]^2 + K_{1,HL}[H]$$

where $V_B$ = volume of titrant (base) added, $V_L$ = initial volume of IRT1pep, $C_L$ = initial concentration of IRT1pep, $K_{HTFA} = 10^{0.30}$, $C_B$ = concentration of titrant (base), and $\beta_{n,HL} = \Pi_{x=1}^{n} K_{x,HL}$.

## Results

Isothermal titration calorimetry (ITC) was used to measure the heat flow associated with metal-ion binding to a 10 residue peptide corresponding to the histidine-rich sequence of IRT1, designated IRT1pep. Except in a few cases, the titrations indicated 1:1 stoichiometry, and the raw data were integrated and fit with a one-site binding model to determine the best-fit values for the experimental stability constant ($K_{ITC}$) and the change in enthalpy associated with the binding reaction ($\Delta H_{ITC}$). Figure 1 shows representative ITC data when 4.2 mM $Zn^{2+}$ is titrated into 0.065 mM IRT1pep at 25 °C, with both solutions identically buffered at pH 7.25 by 25 mM ACES.[21] Table 1 summarizes the best-fit values for the metals investigated in this study. In addition, it contains relevant stabilities and formation enthalpies of metal-buffer complexes, some of which were determined as part of this study.

Because these titrations involve coupled protonation equilibria and buffers that have a measurable interaction with metal ions, thermodynamic cycles were used to determine the pH- and buffer-independent enthalpies and free energies of formation of the metal−peptide complexes from the experimental values. Table 2 shows the cycle for $Zn^{2+}$, which includes the overall equilibrium expression, the individual equilibria involved in $Zn^{2+} \rightarrow$ IRT1pep titrations in ACES buffer, and the coefficients for these equilibria that account for the pH and buffer concentration. The values of $\Delta H^0$ and $\Delta G^0$ for $Zn^{2+}$ binding to IRT1pep (Table 2, eq 8) were determined from the experimental $\Delta H_{ITC}$ and $\Delta G_{ITC}$ values for the overall equilibrium (Table 1), values for the individual equilibria, and coefficients appropriate for the experimental conditions of pH 7.25 and 25 mM ACES ($x = 0.58$, $y = 0.27$, $r = 0.00$, $s = 0.00$, $t = 0.13$, $u = 0.52$). However, several of the individual $\Delta H^0$ and $\Delta G^0$ values necessary for these cycles were not available in the literature and had to be determined as part of this study, as described below.

The enthalpies of formation of certain metal−buffer complexes were determined with ITC titrations involving

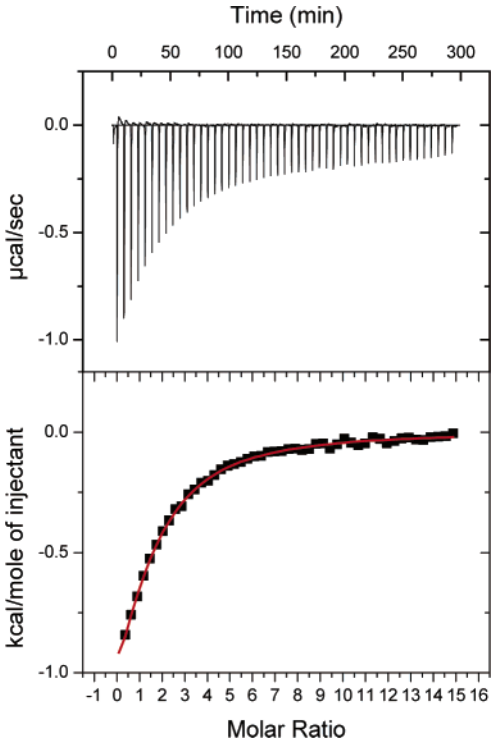


**Figure 1.** ITC titration of 4.2 mM $ZnCl_2$ into 0.065 mM IRT1pep at 25 °C buffered by 25 mM ACES at pH 7.25; solid line is the best fit with a one-site model and the values $n = 1.07 \pm 0.02$, $K_{ITC} = 8.6 \pm 0.4 \times 10^3$, and $\Delta H_{ITC} = -2.3 \pm 0.2$ kcal/mol.

EDTA displacement of the buffer, because the formation enthalpies of metal−EDTA complexes are accurately known.[22] The metal−buffer complex was titrated into an identically buffered EDTA solution, using pH, ionic strength, and concentrations of the metal and buffer that were identical to those used in the IRT1pep titrations. Analysis of these data provides the total heat of metal dissociation from the buffer for these experimental conditions (Table 1).[23]

Deprotonation and protonation equilibria contribute to the overall equilibrium expressions (Table 2) and affect both the experimental enthalpy ($\Delta H_{ITC}$) and binding constant ($K_{ITC}$). To fully characterize the thermodynamics of metal binding, we must know the number of protons displaced from the peptide by metal ions. Two complimentary methods were used to determine this value.

The first is a calorimetric method[24] based on the experimental enthalpy relationship

$$\Delta H_{ITC} = n(\Delta H_{HBuff} - \Delta H_{H-IRT1pep}) - m(\Delta H_{MBuff} + \Delta H_{M-IRT1pep}) \quad (3)$$

where $\Delta H_{HBuff}$, $\Delta H_{MBuff}$, $\Delta H_{H-IRT1pep}$ and $\Delta H_{M-IRT1pep}$ are heats associated with proton and metal binding to the buffer and IRT1pep, and $n$ is the average number of $H^+$ that are

(21) The early portions of the $Zn^{2+} \rightarrow$ peptide titrations (Figure 1, top) have small endothermic peaks, the magnitude of which correlate inversely with the stability of the Zn−buffer complex(es). Although control ($Zn^{2+}$ dilution) titrations in weakly coordinating buffers are also endothermic and have a similar decaying titration profile, careful analysis of the injection peak magnitude and particularly its shape, which reflects the kinetics to establish equilibrium, suggests that these are due to metal solution chemistry unrelated to dilution or binding to the peptide. They were excluded from the integrated heat of reaction, which may lead to a small underestimation of $\Delta H_{ITC}$.

(22) *NIST Standard Reference Database 46*, version 7.0; National Institute of Standards and Technology: Gaithersburg, MD, 2003.

(23) The values for individual metal−buffer species cannot be determined when more than one is present; for cases involving 1:1 and 1:2 metal−buffer complexes, it was assumed that the formation enthalpy of the latter is twice that of the former.

(24) Doyle, M. L.; Louie, G.; Dal Monte, P. R.; Sokoloski, T. D. In *Methods in Enzymology*; Academic: New York, 1995; Vol. 259, pp 183−194.

**Table 1.** Best Fit Values of $K_{ITC}$ and $\Delta H_{ITC}$ from ITC Data, and Metal−Buffer Stability Constants and Formation Enthalpies (errors in best-fit values are listed in parentheses)

| metal | buffer | $K_{ITC}$ | $\Delta H_{ITC}$ (kcal/mol) | log $K_{1,MBuff}$ | log $\beta_{2,M(Buff)2}$[a] | $\Delta H^0_{MBuff}$[b] (kcal/mol) |
|---|---|---|---|---|---|---|
| $Fe^{2+}$ | MOPS[c] | 311 (4) | −4.47 (0.04) | 1.14[b] | | −1.61 (0.01) |
| $Co^{2+}$ | PIPES[c] | 2930 (60) | −7.3 (0.1) | 1.65[b] | | −0.0191 (0.0004) |
| | Tris[d] | 1750 (190) | | 1.73[a] | | |
| $Ni^{2+}$ | ACES[c] | 2580 (50) | −9.1 (0.2) | 3.12[a] | 5.43 | −7.914 (0.004) |
| | Tris[d] | 21 900 (580) | | 2.63[a] | 4.6 | |
| $Cu^{2+}$ | ACES[c] | 14 400 (348) | −6.4 (0.1) | 4.33[a] | 7.77 | −11.5 (0.2) |
| $Zn^{2+}$ | ACES[c] | 8610 (255) | −2.34 (0.09) | 2.34[a] | 3.74 | −4.7 (0.1) |
| | Tris[d] | 17 300 (760) | | 2.27[a] | | |
| $Cd^{2+}$ | ACES[c] | 2790 (29) | −7.65 (0.04) | 1.75[a] | 2.96 | −3.2040 ($1 \times 10^{-4}$) |
| | Tris[d] | 1940 (67) | | 1.88[a] | | |
| $Fe^{3+}$[e] | IRT1pep | $3.13 \times 10^6$ ($1.72 \times 10^5$) | −7.44 (0.04) | | | |

[a] See ref 22. [b] Determined by ITC measurement of buffer displacement by trien or EDTA. [c] pH 7.25. [d] pH 8.22. [e] Determined by EDTA displacement of peptide at pH 6.45 (see text).

**Table 2.** Thermodynamic Cycle for $Zn^{2+} \rightarrow$ IRT1pep Calorimetric Experiments

| eq | reaction | coeff[a] | $\Delta H^0$ (kcal/mol) | $\Delta G^0$ (kcal/mol) |
|---|---|---|---|---|
| | $x$Zn(ACES)$^+$ + $y$Zn(ACES)$_2$ + $(1-x-y)$$Zn^{2+}$ + $(1-r-s-t-u)$IRT1pep + $r$$H_4$IRT1pep$^{4+}$ + $s$$H_3$IRT1pep$^{+3}$ + $t$$H_2$IRT1pep$^{+2}$ + $u$HIRT1pep$^+$ + $(4r+3s+2t+u-2y-x)$ACES$^-$ ⇄ ZnIRT1pep$^{+2}$ + $(4r+3s+2t+u)$HACES | | −2.34[b] | −5.37[b] |
| 1 | Zn(ACES)$^+$ ⇄ $Zn^{2+}$ + ACES$^-$ | $x$ | 4.19[e] | 4.25[c] |
| 2 | Zn(ACES)$_2$ ⇄ $Zn^{2+}$ + 2ACES$^-$ | $y$ | 8.37[e] | 7.4[c] |
| 3 | $H_4$IRT1pep$^{4+}$ ⇄ $H_3$IRT1pep$^{+3}$ + $H^+$ | $r$ | 7.10[c,d] | 4.69[e] |
| 4 | $H_3$IRT1pep$^{+3}$ ⇄ $H_2$IRT1pep$^{+2}$ + $H^+$ | $r+s$ | 7.10[c,d] | 7.27[e] |
| 5 | $H_2$IRT1pep$^{+2}$ ⇄ HIRT1pep$^+$ + $H^+$ | $r+s+t$ | 7.10[c,d] | 9.07[e] |
| 6 | HIRT1pep$^+$ ⇄ IRT1pep + $H^+$ | $r+s+t+u$ | 7.10[c,d] | 10.13[e] |
| 7 | $H^+$ + ACES$^-$ ⇄ HACES | $4r+3s+2t+u$ | −9.34[c] | −9.29[c] |
| 8 | $Zn^{+2}$ + IRT1pep ⇄ ZnIRT1pep$^{+2}$ | 1 | −5.87[f] | −9.13[f] |

[a] Coefficients are pH-dependent values accounting for peptide protonation speciation ($r-u$) and metal−buffer speciation ($x$, $y$), which also depends on buffer concentration. [b] From Table 1. [c] See ref 22. [d] Histidine enthalpy of deprotonation. [e] Determined in this study. [f] Determined from this cycle.

displaced from the peptide when $m$ metal ions bind. In this case, $m = 1$. Carrying out metal → IRT1pep titrations at constant pH and ionic strength but varying the buffer results in values of $\Delta H_{ITC}$ that depend on $n$ and known values for the metal−buffer interaction enthalpy and the buffer protonation enthalpy, leading to a linear relationship, eq 4, from which $n$ can be determined.

$$\Delta H_{ITC} + \Delta H_{MBuff} = n(\Delta H_{HBuff}) + (\Delta H_{M-IRTpep} - n\Delta H_{H-IRTpep}) \quad (4)$$

Figure 2 shows a plot of these data for $Zn^{2+} \rightarrow$ IRT1pep titrations, which has a slope of $n = 0.79 \pm 0.02$, quantifying the number of protons that are displaced at pH 7.25. In addition, the $y$-intercept of this plot, 0.21 ± 0.08 kcal/mol, is the enthalpy of $Zn^{2+}$ coordination minus the protonation enthalpy for the 0.8 protons displaced from IRT1pep at this pH. Assuming that these 0.8 protons are displaced from the histidines, it can be estimated that $\Delta H_{Zn-IRTpep} = -6.0$ kcal/mol, a value in excellent agreement with the −5.87 kcal/mol determined by the thermodynamic cycle (Table 2).

The second method, which assumes that protons are displaced from the histidines by the metal ion, requires the p$K_a$'s of the His residues of IRT1pep. These were determined by fitting a pH titration of the peptide (see the Supporting Information) to an algorithm appropriate for this system, as described in the Experimental Section. The experimental p$K_a$ values[25] are 3.44 ± 0.03, 5.32 ± 0.04, 6.65 ± 0.04, and 7.43 ± 0.06, and provide a value of $n = 0.79 \pm 0.09$ at pH 7.25, in excellent agreement with the value obtained calorimetrically.

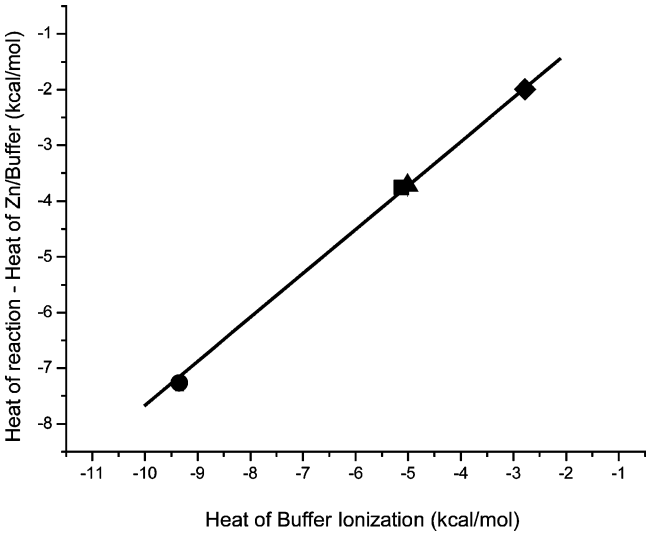


**Figure 2.** Calorimetric determination of $H^+$ displaced from IRT1pep upon $Zn^{2+}$ binding at pH 7.25 (see text); enthalpies (kcal/mol) used for values in the plot are ACES (circle): $\Delta H_{ITC} = -2.34$, $\Delta H_{ZnACES} = -4.71$, $\Delta H_{H-ACES} = -9.34$; HEPES (square): $\Delta H_{ITC} = -3.25$, $\Delta H_{ZnHEPES} = -0.29$, $\Delta H_{H-HEPES} = -5.12$; MOPS (triangle): $\Delta H_{ITC} = -3.42$, $\Delta H_{ZnMOPS} = -0.09$, $\Delta H_{H-MOPS} = -5.01$; PIPES (diamond): $\Delta H_{ITC} = -1.99$, $\Delta H_{ZnPIPES} = +0.22$, $\Delta H_{H-PIPES} = -2.78$; linear regression values: $b = 0.79 \pm 0.02$, $a = 0.21 \pm 0.08$, $r = 0.999$.

The ferric ion presents a unique challenge for these experiments. Unlike the other metals, it was not possible to solubilize enough $Fe^{3+}$ to generate a measurable amount of heat when titrations were carried out at reasonable buffer concentrations.[26] This problem was overcome by preparing an $Fe^{3+}$ solution buffered by IRT1pep at pH 6.45, where it

**Table 3.** Thermodynamic Cycle for EDTA/IRT1pep → $Fe^{3+}$/IRT1pep Calorimetric Experiments

| eq | reaction | coeff[a] | $\Delta H^0$ (kcal/mol) | $\Delta G^0$ (kcal/mol) |
|---|---|---|---|---|
| | $FeIRT1pep^{+3} + xH_2EDTA^{-2} + (1-x)HEDTA^{-3} + \{(1+q)(r+s+t) - 1\}IRT1pep \rightleftarrows (1-z)FeEDTA^{-} + zFe(OH)EDTA^{-2} + r(1+q)HIRT1pep^{+} + s(1+q)H_2IRT1pep^{+2} + t(1+q)H_3IRT1pep^{+3}$ | | −7.44[b] | −8.86[b] |
| 1 | $H_2EDTA^{-2} \rightleftarrows HEDTA^{-3} + H^{+}$ | $x$ | 4.2[c] | 8.36[c] |
| 2 | $HEDTA^{-3} \rightleftarrows EDTA^{-4} + H^{+}$ | 1 | 5.4[c] | 12.98[c] |
| 3 | $FeIRT1pep^{+3} \rightleftarrows Fe^{+3} + IRT1pep$ | 1 | −1.3[e] | 22.45[e] |
| 4 | $Fe^{3+} + EDTA^{-4} \rightleftarrows FeEDTA^{-}$ | 1 | −2.7[c] | −34.26[c] |
| 5 | $FeEDTA^{-} \rightleftarrows Fe(OH)EDTA^{-2} + H^{+}$ | $z$ | 10[c] | 10.08[c] |
| 6 | $IRT1pep + H^{+} \rightleftarrows HIRT1pep^{+}$ | $(1+q)(r+s+t)$ | −7.10[c,d] | −10.13[f] |
| 7 | $HIRT1pep^{+} + H^{+} \rightleftarrows H_2IRT1pep^{+2}$ | $(1+q)(s+t)$ | −7.10[c,d] | −9.07[f] |
| 8 | $H_2IRT1pep^{+2} + H^{+} \rightleftarrows H_3IRT1pep^{+3}$ | $(1+q)t$ | −7.10[c,d] | −7.27[f] |

[a] Coefficients are pH-dependent values accounting for protonation speciation (the $(1+q)$ term accounts for $H_yIRT1pep$ buffering and is calculated by setting $H^{+}_{consumed} = H^{+}_{produced}$). [b] From Table 1. [c] See ref 22. [d] Histidine enthalpy of protonation. [e] Determined from this cycle. [f] Determined in this study.

was found that 5.0 mM IRT1pep solubilized ~6 $\mu$M $Fe^{3+}$.[27] EDTA, in a 5.0 mM IRT1pep solution at pH 6.45, was titrated into an identical IRT1pep solution with solubilized $Fe^{3+}$, generating the ITC data in Figure 3. A unique thermodynamic cycle was constructed to analyze these data, as outlined in Table 3, with coefficients appropriate for the experimental conditions ($x = 0.323$, $z = 0.103$, $q = -0.115$, $r = 0.564$, $s = 0.043$, $t = 0.0$).

Figure 4 shows the ITC data for an $Fe^{2+}$ → IRT1pep titration, which indicates a low affinity of the peptide for the ferrous ion. Although the stability constant from a fit of these data lies outside the normal range for titration calorimetry, as quantified by the $c$ value,[28] several favorable experimental criteria,[29] including accurately known concentrations of all species, a sufficient signal-to-noise ratio, and an extended reaction profile, allowed for an accurate determination of $K_{ITC}$ and $\Delta H_{ITC}$ associated with this complex, whose stability is lower than that of other metal ions (Table 1).

Evidence for $Mn^{2+}$ coordination to the peptide was not detected by ITC, because of the low stability of the complex and/or negligible net heat associated with binding, but was observed by EPR spectroscopy. Figure 5 compares the 77 K EPR spectra of 1.0 mM $MnCl_2$ in 50% glycerol to that of 1.0 mM $MnCl_2$ in the presence of 1.0 mM IRT1pep. Significant broadening of the $Mn^{2+}$ signal in the presence of the peptide provides evidence of $Mn^{2+}$ binding to

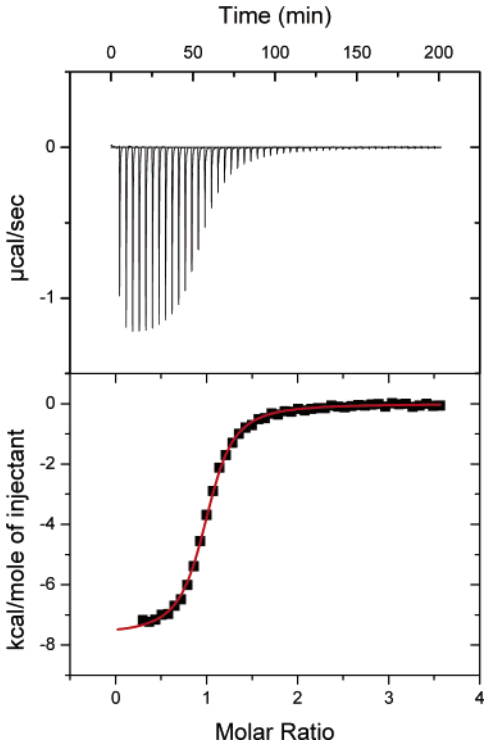


**Figure 3.** ITC titration of 1.0 mM EDTA into 6.5 $\mu$M $Fe^{3+}$ at 25 °C buffered by 5.0 mM IRT1pep at pH 6.45; solid line is the best fit with a one-site model and the values $n = 0.98 \pm 0.003$, $K_{ITC} = 3.1 \pm 0.3 \times 10^6$, and $\Delta H_{ITC} = -7.4 \pm 0.1$ kcal/mol.

IRT1pep. The stability and thermodynamics of a putative Mn−IRT1pep complex were estimated from comparisons with data for trien, which coordinates metals with two primary and two secondary amines and has metal binding properties that parallel those of IRT1pep. Thus, the following relationships

$$\frac{\Delta G_{MnTrien}}{\Delta G_{MTrien}} = \Delta G_{MnIRT1pep}\left(\frac{1}{\Delta G_{MIRT1pep}}\right) \quad (5)$$

$$\frac{\Delta H_{MnTrien}}{\Delta H_{MTrien}} = \Delta H_{MnIRT1pep}\left(\frac{1}{\Delta H_{MIRT1pep}}\right) \quad (6)$$

can be used with known thermodynamic values for $Mn^{2+}$ and other metal ions ($M^{+2}$) binding to trien[22] and values determined for IRT1pep in this study to quantify $\Delta H_{MnIRT1pep}$ and $\Delta G_{MnIRT1pep}$.

(25) The fitting algorithm for the titration data includes five p$K_a$ values that correspond to the four histidine residues, as reported in the text, and the C-terminal amide. These values are macroscopic p$K_a$'s and are therefore dependent on the electrolytic environment. Although p$K_a$ values are not available for a peptide containing four histidines, values have been determined for H−(His−Gly)$_2$−OMe (5.33 and 6.37) and H−(His−Gly)$_2$−OH (5.33 and 6.55): Casolaro, M.; Chelli, M.; Ginanneschi, M.; Laschi, F.; Muniz-Miranda, M.; Papini, A. M.; Sbrana, G. *Spectrochim. Acta, Part A* **1999**, *55*, 1675−1689.

(26) For a constant ionic strength to be maintained ($I = 0.1$ M), the buffer concentration cannot exceed a threshold value dictated by pH and buffer contribution to the ionic strength.

(27) Using these values of pH, [IRT1pep], [$Fe^{3+}_{solubilized}$], and the $K_{sp}$ of $Fe(OH)_3$, we can estimated a value for $K_{FeIRT1pep}$; it is found to be in reasonable agreement with the value determined by calorimetry.

(28) Defined as $c = nK$[macromolecule], where $1 < c < 1000$ is generally required to obtain a unique value of $K$ from fits of ITC data. Wiseman, T.; Williston, S.; Brandts, J. F.; Lin, L. *Anal. Biochem.* **1989**, *179*, 131−137.

(29) Turnbull, W. B.; Daranas, A. H. *J. Am. Chem. Soc.* **2003**, *125*, 14859−14866.

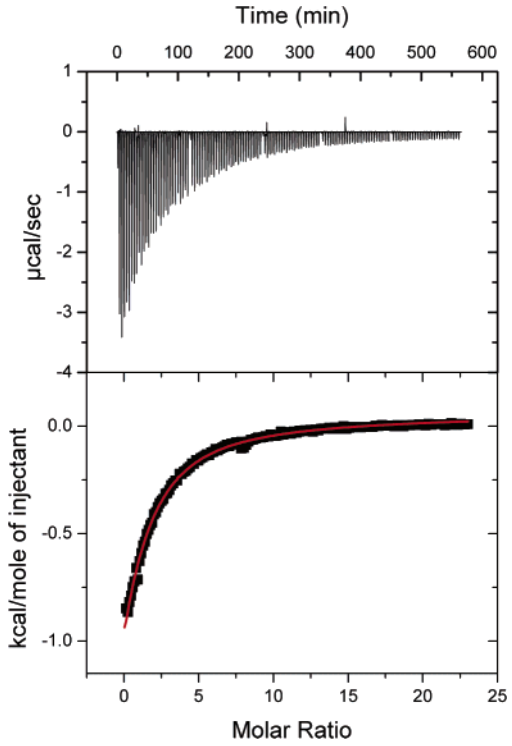


**Figure 4.** ITC titration of 12.5 mM $Fe^{2+}$ into 0.85 mM IRT1pep at 25 °C buffered by 25 mM MOPS at pH 7.25 under strict anaerobic conditions; raw data of four sequential experiments were concatenated (see Experimental Section) to generate the binding profile; solid line is the best fit with a one-site model assuming 1:1 stoichiometry ($n$ fixed at 1.0) and the values $K_{ITC} = 311 \pm 7$ and $\Delta H_{ITC} = -4.47 \pm 0.06$ kcal/mol.

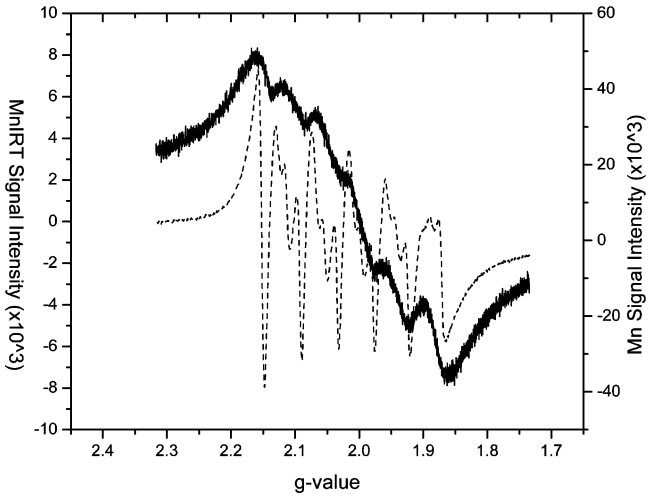


**Figure 5.** Frozen solution (77 K) EPR spectra of 1.0 mM $MnCl_2$ in 50% glycerol (dashed line) and 1.0 mM $MnCl_2$ with 1.0 mM IRT1pep (solid line).

Table 4 shows the pH- and buffer-independent thermodynamic values for metal ions binding to IRT1pep. This includes log $K$ (and $\Delta G^0$) values for $Co^{2+}$, $Ni^{2+}$, $Zn^{2+}$, and $Cd^{2+}$ from ITC data obtained in Tris buffer at pH 8.22, in addition to data with various buffers at pH 7.25. The close match of values obtained under different conditions suggests that pH- and buffer-dependent contributions have been eliminated. The absence of a value for $Cu^{2+}$ at pH 8.22 in 100 mM Tris is due to the high stability of the $Cu(Tris)_4^{+2}$ complex (log $\beta_4 = 14.1$).[22]

**Table 4.** Summary of pH- and Buffer-Independent Thermodynamic Values for Metal-Ion Binding to IRT1pep Determined from Data Collected at 298 K and pH 7.25 (values in parentheses indicate associated error)

| metal | log $K$ | $\Delta G^0$ (kcal/mol)[a] | $\Delta H^0$ (kcal/mol) | $\Delta S^0$ (cal mol$^{-1}$ K$^{-1}$)[b] |
|---|---|---|---|---|
| $Mn^{2+}$ | 1.3 (48) | −1.72 (36)[c] | −2 (28)[c] | −1.76 (31) |
| $Fe^{2+}$ | 2.82 (0.66) | −3.85 (1.10) | −6.49 (0.73) | −8.9 (4.2) |
| $Co^{2+}$ | 4.46 (0.41) | −6.08 (1.09) | −10.39 (0.66) | −14.5 (4.1) |
| | 4.44 (0.12)[d] | −6.06 (0.32) | | |
| $Ni^{2+}$ | 8.70 (0.30) | −11.86 (1.67) | −15.89 (1.71) | −13.5 (7.8) |
| | 8.49 (0.14)[d] | −11.59 (0.69) | | |
| $Cu^{2+}$ | 12.25 (0.28) | −16.70 (2.05) | −16.76 (2.13) | −0.2 (9.9) |
| $Zn^{2+}$ | 6.69 (0.25) | −9.13 (1.00) | −5.89 (0.88)[e] | 10.9 (4.3) |
| | 6.21 (0.09)[d] | −8.47 (0.33) | | |
| $Cd^{2+}$ | 4.99 (0.33) | −6.80 (0.97) | −9.71 (0.80) | −9.8 (4.0) |
| | 4.71 (0.14)[d] | −6.43 (0.38) | | |
| $Fe^{3+}$ | 16.54 (0.13)[f] | −22.45 (1.24) | 1.29 (1.00)[f] | 80.0 (5.2) |

[a] $\Delta G^0 = -RT \ln K$. [b] $\Delta S^0 = -(\Delta G^0 - \Delta H^0)/T$. [c] From estimated values (see text). [d] From data collected at pH 8.22 with 100 mM Tris buffer. [e] See ref 30. [f] From data collected at pH 6.45.

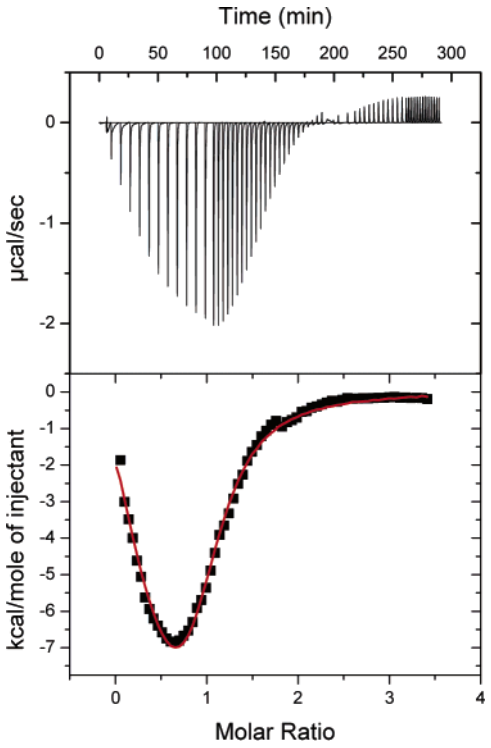


**Figure 6.** ITC titration of 1.0 mM IRT1pep into 0.10 mM $Cu^{2+}$ at 25 °C buffered by 25 mM PIPES at pH 7.25; solid line is the best fit with a sequential binding model and the values $K_{1ITC} = 2.5 \pm 0.1 \times 10^5$, $\Delta H_{1ITC} = -10.5 \pm 0.9$ kcal/mol, $K_{2ITC} = 1.29 \pm 0.09 \times 10^4$, $\Delta H_{2ITC} = 9.5 \pm 0.3$ kcal/mol; designating $Cu^{2+}$, which is in the cell, as the "ligand" assigns $K_2$ and $\Delta H_2$ to the first event at $n = 0.5$ (formation of the 2:1 complex).

Only for $Cu^{2+}$ was there clear evidence for metal−peptide species other than the 1:1 complex and then only with weakly coordinating buffers. Figure 6 shows ITC data for an IRT1pep → $Cu^{2+}$ titration in PIPES, which has a binding profile suggesting initial formation of a $Cu_2$IRT1pep complex, followed by the 1:1 complex. The unexpected endothermic heat of formation of the initial 2:1 complex may indicate a hydroxo-bridged di-$Cu^{2+}$ complex, which would have a large endothermic contribution from deprotonation of $H_2O$ ($\Delta H^0 = 13.50$ kcal/mol[22]). Because of the low solubility of $Cu^{2+}$ in PIPES, the forward titration ($Cu^{2+}$ →

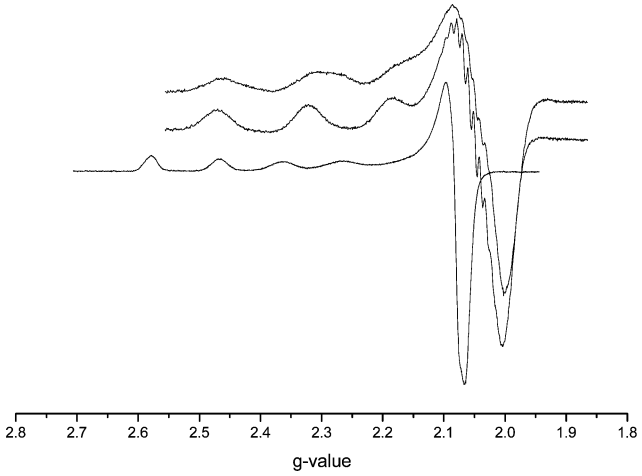


**Figure 7.** Frozen solution (77 K) EPR spectra of (bottom) 1.0 mM $Cu^{2+}$ in 50% glycerol ($g_{||} = 2.413$, $A_{||} = 137 \times 10^{-4}$ cm$^{-1}$, $g_{\perp} = 2.085$), (middle) 1.0 mM $Cu^{2+}$ in 1.0 mM IRT1pep ($g_{||} = 2.250$, $A_{||} = 189 \times 10^{-4}$ cm$^{-1}$, $g_{\perp} = 2.049$, $A_{\perp} = 13.2 \times 10^{-4}$ cm$^{-1}$), and (top) 1.0 mM $Cu^{2+}$ in 0.5 mM IRT1pep.

IRT1pep) could not be performed, limiting our ability to confirm this interaction. However, forward titrations in HEPES buffer show evidence of an initial 1:2 complex, Cu(IRT1pep)$_2$, early in the titration when there is an excess of IRT1pep, followed by the net endothermic formation of the 1:1 complex.

The presence of multiple $Cu^{2+}$−IRT1pep species during ITC titrations in the absence of strongly coordinating buffer is supported by the EPR spectra in Figure 7. The spectrum of the 1:1 complex shows nine clearly-resolved superhyperfine lines in the perpendicular region, indicative of four His imidazoles ($^{14}$N, $I = 1$) coordinating in the equatorial plane of the $Cu^{2+}$, and three clearly-resolved hyperfine lines of the four expected for $^{63,65}$Cu ($I = 3/2$) in the parallel region. By comparison, the EPR spectrum of a sample with a 2:1 ratio of $Cu^{2+}$ to IRT1pep has a $g_{\perp}$ value similar to that of the 1:1 complex, poorly resolved superhyperfine lines, and significantly broadened hyperfine features that do not match those of $Cu^{2+}$(aq), indicating multiple Cu−peptide species, as predicted by the ITC-measured stability constants, with different $Cu^{2+}$ coordination.

## Discussion

Although metal uptake by IRT1 and other members of the ZIP family of metal transporters has been well-studied, the role of the striking His-rich sequences in these proteins is still poorly understood. The goal of this study was to quantify the thermodynamics of metal binding to a peptide corresponding to this sequence in IRT1, and thereby provide fundamental chemical insight relevant to its potential role(s) in metal uptake by this transmembrane protein.

**Chemistry.** The peptide binds metal ions with the relative affinity $Fe^{3+} > Cu^{2+} > Ni^{2+} > Zn^{2+} > Cd^{2+} \approx Co^{2+} > Fe^{2+} \approx Mn^{2+}$ and with the thermodynamics quantified in Table 4. Useful comparisons can be made between this tetraimidazole polydentate peptide and the well-characterized tetramine ligand trien. The free energies and enthalpies (Figure 8) of both IRT1pep and trien binding to dipositive

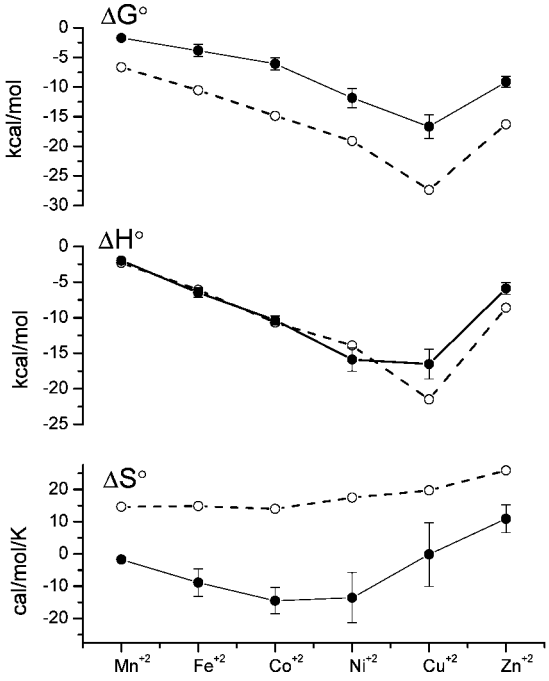


**Figure 8.** Thermodynamic values for dipositive metal ions coordinating to IRT1pep (solid circles and lines) and trien[22] (empty circles and dashed lines); error bars associated with $Mn^{2+}$ are not shown because of their magnitude.

first-row transition-metal ions are consistent with the Irving−Williams series,[31] which predicts an increase in stability from $Mn^{2+}$ to $Cu^{2+}$, followed by a lower stability for $Zn^{2+}$. This trend is explained by contributions from ionic and covalent character in the metal−ligand bonding[32] and is generally found in cases such as IRT1pep and trien with neutral amines, which are intermediate ligands in the hard−soft acid−base (HSAB) classification.

Although the coordination enthalpies (Figure 8, middle) for IRT1pep and trien are very similar, reflecting their common nitrogen ligation, the trien complexes are quantitatively more stable, as indicated by the coordination free energies (Figure 8, top). The origin of this difference is the coordination entropy (Figure 8, bottom), which is less favorable for IRT1pep. For trien, there is a small increase in coordination entropy with increasing atomic number, except for $Co^{2+}$, whereas the values for IRT1pep decrease from $Mn^{2+}$ to $Ni^{2+}$ followed by an increase for $Cu^{2+}$ and $Zn^{2+}$. However, considering the uncertainty (error bars) associated with the IRT1pep $\Delta S^0$ values, particularly those estimated for $Mn^{2+}$, the trend for the peptide data is not inconsistent with that of trien.

A dominant contribution to the entropy of formation of metal complexes is the release of water that is coordinated (inner sphere) and ordered (outer sphere) by the metal ion.[33]

(30) The enthalpy value reported here may be a low estimate because of small endothermic features that could affect the magnitude of the exothermic peaks; this is corroborated by the reverse titration in HEPES buffer, where $\Delta H^0$ is found to be $-6.2 \pm 0.9$ kcal/mol, leading to $\Delta S^0 = 4.8 \pm 1.4$ cal mol$^{-1}$ K$^{-1}$.

(31) Irving, H.; Williams, R. J. P. *Nature* **1948**, *162*, 746−747.

(32) Gorelsky, S. I.; Basumallick, L.; Vura-Weis, J.; Sarangi, R.; Hodgson, K. O.; Hedman, B.; Fujisawa, K.; Solomon, E. I. *Inorg. Chem.* **2005**, *44*, 4947−4960.

**Table 5.** Metric Data for Transition Metal Ions

| metal | 4-coordinate ionic radius (Å)[a] | 6-coordinate ionic radius (Å)[a] | $H_2O$ in 2nd hydration sphere | average M−N bond length (Å)[e] |
|---|---|---|---|---|
| $Mn^{2+}$ | 0.80 | 0.97 | | 2.326 |
| $Fe^{2+}$ | 0.77 | 0.92 | 12.4[b] | 2.255 |
| $Co^{2+}$ | 0.72 | 0.88 | 12.7[d] | 1.966 |
| $Ni^{2+}$ | 0.69 | 0.83 | 13.4[d] | 2.068 |
| $Cu^{2+}$ | 0.71 | 0.87 | 13.2[c] | 2.045 |
| $Zn^{2+}$ | 0.74 | 0.88 | 12.2[d] | 2.158 |

[a] See ref 39. [b] See ref 40. [c] See ref 42. [d] See ref 41. [e] See ref 43.

The first shell coordination number is six for these metal ions,[34] but five for $Cu^{2+}$.[35−38] Numbers of waters in the second hydration sphere are also available (Table 5), and these inversely correlate with the ionic radius. Although the final complex with neutral N-donor ligands also has a dipositive charge, differences in metal charge density are modulated by the ligand and may be similar for the metal−ligand species. Thus, the entropy of complex formation is expected to increase modestly from $Mn^{2+}$ to $Ni^{2+}$, which, except for $Co^{2+}$, is what is observed. However, $Co^{2+}$ has somewhat shorter than expected metal−nitrogen bond lengths (Table 5), resulting in more rigidly constrained complexes that may correlate with the slightly lower than expected coordination entropy.

Although the ionic radius increases, and number of second hydration sphere waters decreases, from $Ni^{2+}$ to $Cu^{2+}$ to $Zn^{2+}$, the net coordination entropy increases. For $Cu^{2+}$, this may be due to Jahn−Teller distortions of the metal−ligand complex and a resulting higher conformational entropy. The final $Zn^{2+}$ complex is also expected to have greater conformational flexibility (entropy) because of longer Zn−N bond lengths (Table 5). Thus, loss of ordered water from the metal ion and conformational entropy of the resulting metal−ligand complex appears to correlate with the observed trend in coordination entropy for trien and IRT1pep.

Because trien and IRT1pep have parallel periodic trends in their coordination entropies, this suggests that the quantitative difference is predominantly due to a specific contribution. For the reaction

$$M(H_2O)_6^{+2} + N_4Lig \rightleftarrows MN_4Lig^{+2} + 6\,H_2O \qquad (7)$$

where $N_4Lig$ represents IRT1pep or trien, the major entropic contributions are expected to be (a) displacement of water from the metal, (b) metal coordination to the ligand, (c) displacement of solvation around each nitrogen of the ligand, and (d) conformational constraint of the coordinated ligand. For both IRT1pep and trien, the entropic contributions should be identical or similar for the first three. Therefore, the difference in coordination entropy between the peptide and trien, $\Delta\Delta S^0_{average} = -22.3 \pm 1.6$ cal mol$^{-1}$K$^{-1}$, appears to be largely due to the difference in loss of conformational degrees of freedom. Compared to trien, IRT1pep is considerably more flexible and $\Delta\Delta S^0$ predominantly reflects a greater loss of conformational entropy upon complex formation.

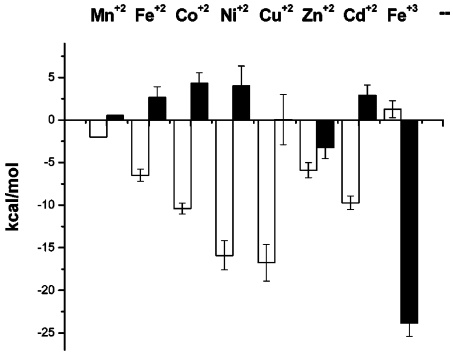


**Figure 9.** Enthalpic ($\Delta H^0$, empty columns) and entropic ($-T\Delta S^0$, solid columns) contributions to the free energy of metal binding to IRT1pep. Error bars associated with Manganese were excluded because of their magnitude.

Figure 9 provides a useful summary of the relative enthalpic and entropic contributions to the binding of metal ions to ITR1pep. The Irving−Williams series is graphically displayed by the enthalpic component, which is the major contributor to the trend in stability of this series. $Fe^{3+}$ binding to IRT1pep is unique among the metal ions studied because it is entirely due to a favorable net entropy of coordination. A large entropy term is common for $Fe^{3+}$ coordination chemistry[22,44,45] and can be rationalized by the $Fe^{3+}$ heat of hydration, $\Delta H^0_{hydration} = -1045$ kcal/mol,[39] which is twice that of the other metal ions studied and leads to a large endothermic dehydration enthalpy. Although $Fe^{3+}$ coordination numbers in the first and second hydration shells (6 and 13.4, respectively[40]) are similar to those of the dipositive metal ions, a stronger interaction with first and second shell waters and solvent ordering beyond the second shell by the tripositive metal ion would lead to both an enthalpic penalty and an entropic gain from the release of coordinated and ordered water upon binding IRT1pep or other ligands.

**Biology.** IRT1, the high affinity iron transporter of *Arabidopsis thaliana* and founding member of the ZIP family of proteins, is upregulated in response to iron-deficient conditions and imports $Fe^{2+}$. It is also able to transport the essential metals $Zn^{2+}$, $Co^{2+}$, and $Mn^{2+}$, but the biological significance of this is not known. However, IRT1 transport of $Cd^{2+}$ is predicted to be one of the major uptake pathways for this toxic metal ion.

(33) Although IRT1pep titrations involve metal−buffer solutions, the thermodynamic cycles used in data analysis account for metal−buffer interactions and therefore reference the aquo metal ion.
(34) Ohtaki, H.; Radnai, T. *Chem. Rev.* **1993**, *93*, 1157−1204.
(35) Frank, P.; Benfatto, M.; Szilagyi, R. K.; D'Angelo, P.; Della Longa, S.; Hodgson, K. O. *Inorg. Chem.* **2005**, *44*, 1922−1933.
(36) Marini, G. W.; Liedl, K. R.; Rode, B. M. *J. Phys. Chem. A* **1999**, *103*, 11387−11393.
(37) Amira, S.; Spangberg, D.; Hermansson, K. *Phys. Chem. Chem. Phys.* **2005**, *7*, 2874−2880.
(38) Pasquarello, A.; Petri, I.; Salmon, P. S.; Parisel, O.; Car, R.; Toth, E.; Powell, D. H.; Fischer, H. E.; Helm, L.; Merbach, A. E. *Science* **2001**, *291*, 856−859.
(39) Holleman, A. F.; Wiberg, E. In *Inorganic Chemistry;* Academic: San Diego, 1995.
(40) Remsungnen, T.; Rode, B. M. *J. Phys. Chem. A* **2003**, *107*, 2324−2328.
(41) D'Angelo, P.; Barone, V.; Chillemi, G.; Sanna, N.; Meyer-Klaucke, W.; Pavel, N. V. *J. Am. Chem. Soc.* **2002**, *124*, 1958−1967.
(42) Schwenk, C. F.; Rode, B. M. *J. Chem. Phys.* **2003**, *119*, 9523−9531.
(43) Allen, F. H. *Acta Crystallogr., Sect. B* **2002**, *58*, 380−388.
(44) Fish, L. L.; Crumbliss, A. L. *Inorg. Chem.* **1985**, *24*, 2198−2204.
(45) Lebedeva, N. S.; Yakubov, S. P.; Vyugin, A. I.; Parfenyuk, E. V. *Thermochim. Acta* **2003**, *404*, 19−24.

It has been shown that metal transport is not impeded in ZRT1[10] or IRT1[12] when histidines in the His-rich sequence are mutated to the noncoordinating amino acid glutamine, indicating that these residues are not essential for the uptake mechanism. Immunofluorescence assays have revealed that these mutations in ZRT1 lead to a more random cellular localization of the protein,[14] suggesting that this motif may play a role in targeting ZRT1 to the cellular membrane.

The expression of IRT1 is regulated by the recently discovered Fe-deficiency-induced transcription factor-1 (FIT1), which is responsible for increased levels of IRT1 protein.[46] However, the mechanism for turning off iron uptake by IRT1 is not known. It may be similar to that found for ZRT1, where $Zn^{2+}$, $Co^{2+}$, or $Cd^{2+}$ induce ubiquitination of a key lysine residue in the large intracellular loop, which triggers endocytosis and eventually protein degradation in the vacuole.[14,47,48] Whether the His-rich sequence, which is located in the same intracellular loop, plays any role is not known, although mutation of the IRT1 histidines to glutamines does not affect protein turnover.[15]

Results from this study show that metal ions transported by IRT1 have low affinities for the His-rich sequence. This suggests that any direct feedback control of uptake by metal coordination to this motif could occur only after higher-affinity $Fe^{2+}$ sites in the cell had become saturated. However, the extremely high affinity of the His-rich sequence for $Fe^{3+}$ suggests another possible mechanism for modulating $Fe^{2+}$ uptake. Accumulation of iron in the cell by IRT1 transport could lead to trace amounts of intracellular $Fe^{3+}$, which would bind to the His-rich sequence and could suppress further iron uptake. Ongoing biophysical studies of the entire IRT1 intracellular loop that contains its His-rich sequence will test this and related hypotheses.

**Acknowledgment.** We thank the Howard Hughes Medical Institute, Dartmouth College, and Dartmouth Medical School for funds to purchase the microcalorimeters, and Dartmouth College (Dartmouth Fellowship to N.E.G.), HHMI (Hughes Biological Sciences Internship to S.A.) and NSF (Grant IBN-0419695 to M.L.G.) for support of this research. We also thank Wayne Casey for help with the EPR measurements and Robert Cantor, Anne Spuches, Harriet Kruszyna, and Callie Schieffer for insightful discussions.

**Supporting Information Available:** Plot of the pH titration of 1.25 mM IRT1pep with 100 $\mu$M NaOH. This material is available free of charge via the Internet at http://pubs.acs.org.

IC0606431

(46) Colangelo, E. P.; Guerinot, M. L. *Plant Cell* **2004**, *16*, 3400−3412.
(47) Gitan, R. S.; Luo, H.; Rodgers, J.; Broderius, M.; Eide, D. *J. Biol. Chem.* **1998**, *273*, 28617−28624.
(48) Gitan, R. S.; Eide, D. J. *Biochem. J.* **2000**, *346*, 329−336.